Mechanically Consistent Model of the 2018 Christmas Volcano-Tectonic Event at Etna

Adriana Iozzia, Gilda Currenti, V Cayol, Alessandro Bonforte, Andrea Cannata, J L Froger

AGU ADVANCING EARTH AND SPACE SCIENCES

Geophysical Research Letters

RESEARCH LETTER
10.1029/2023GL108017

Mechanically Consistent Model of the 2018 Christmas Volcano-Tectonic Event at Etna

A. Iozzia[1,2], G. Currenti[2], V. Cayol[3], A. Bonforte[2], A. Cannata[1,2], and J. L. Froger[4]

[1]Dipartimento di Scienze Biologiche, Geologiche e Ambientali—Sezione di Scienze della Terra, Università degli Studi di Catania, Catania, Italy, [2]Istituto Nazionale di Geofisica e Vulcanologia, Osservatorio Etneo—Sezione di Catania, Catania, Italy, [3]Université Clermont Auvergne, CNRS, IRD, OPGC, Laboratoire Magmas et Volcans, Clermont-Ferrand, France, [4]Université Jean Monnet—Faculté des Sciences et Techniques, Laboratoire de géologie de Lyon: Terre, Planètes, Environnement—UMR, CNRS 5276 LGL-TPE, Saint-Etienne, France

Abstract The interaction between volcanic activity and flank instability during the Christmas Eve eruption at Mount Etna in 2018 is explored, using a mechanically consistent inverse model fitting high spatial resolution SAR data. Inversions search for fractures that may be curved and can accommodate co-eval pressure and shear stress changes. Displacements associated with the eruption result from the interaction between two intrusion sources: a buried dyke and a curved sheared intrusion that fed the eruption. Moreover, we identify that the sheared magmatic intrusion induced the observed eastward slip on the Pernicana fault, while the Fiandaca fault was undergoing stress accumulation, which was suddenly released during a M5.0 seismic event. The Fiandaca fault is determined to be listric, rooting beneath the mobile eastern flank of the volcano. This study highlights the role of curved fractures, acting as sheared intrusions or as faults, in volcanoes exhibiting flank instabilities.

Plain Language Summary In this study, we thoroughly examine how volcanic activity and flank dynamics interacted during the 2018 eruption of Mount Etna. We use high-resolution satellite SAR data and a model considering complex mechanical aspects of the volcano's behavior. Formal inversions reveal that the eruption is triggered by the interplay between two intrusion sources: a buried dyke and a curved sheared intrusion, consistent with the earthquake pattern. This study emphasizes the significant role of curved sheared intrusions and faults at volcanoes prone to flank instabilities. Furthermore, we quantify how summit magmatic intrusions promote fault slip in the eastern flank of Etna. These findings differ from previous research that used simpler approaches. In summary, our study provides a new insight into how volcanoes like Etna can erupt and trigger flank slip, shedding light on the complex interactions between magma and tectonics.

Key Points:

- Modeling shows that the magma intrusion feeding the 2018 eruption accommodated coeval opening and shear displacements
- Both the summit intrusions and the Fiandaca fault are curved, probably connected to the detachment at the base of the mobile eastern sector
- The Fiandaca fault was previously locked. It released accumulated stress, while the Pernicana fault passively responded to the intrusion

Supporting Information:

Supporting Information may be found in the online version of this article.

Correspondence to:

A. Iozzia and G. Currenti,
adriana.iozzia@ingv.it;
adriana.iozzia@phd.unict.it;
gilda.currenti@ingv.it

Citation:

Iozzia, A., Currenti, G., Cayol, V., Bonforte, A., Cannata, A., & Froger, J. L. (2024). Mechanically consistent model of the 2018 Christmas volcano-tectonic event at Etna. *Geophysical Research Letters*, *51*, e2023GL108017. https://doi.org/10.1029/2023GL108017

Received 9 JAN 2024
Accepted 2 MAY 2024

Author Contributions:

Conceptualization: A. Iozzia, G. Currenti, V. Cayol, A. Bonforte, A. Cannata
Data curation: J. L. Froger
Formal analysis: A. Iozzia, G. Currenti, V. Cayol
Investigation: A. Iozzia, G. Currenti, V. Cayol
Methodology: A. Iozzia, G. Currenti, V. Cayol
Software: V. Cayol
Supervision: G. Currenti, V. Cayol, A. Bonforte, A. Cannata

1. Introduction

Flank collapses are one of the main hazards in volcanic areas as they can trigger tsunamis and large earthquakes, which together account for 24% of the fatalities at volcanoes (Auker et al., 2013). For shield volcanoes hosting well defined intrusion zones (rift-zones), such as Kilauea, Piton de la Fournaise, and Etna, the stability of volcano flanks and the persistence of magma intrusions result from a balance between volcano activity, gravity, and fault friction (Dieterich, 1988; Iverson, 1995). The different tectonic and geological contexts of these volcanoes lead to different flank slip dynamics resulting from different stress balances. For example, at Kilauea (Hawaii), flank displacement is continuously taking place at a steady rate of 8 cm/year (Miklius et al., 2005), sometimes accelerating during slow slip events (Montgomery-Brown et al., 2015) or large earthquakes, such as the M7.2 1975 (Owen & Bürgmann, 2006) or the M7.0 2018 (Butler, 2019). Flank slip is mainly driven by magma intrusions in the rift zones (Cayol et al., 2000; Dieterich, 1988; Iverson, 1995), along with gravitational spreading (Denlinger & Morgan, 2014), and resisted by gravity and friction along a decollement surface (low angle reverse fault). At Piton de la Fournaise, flank instability was first observed in 2007 when up to 1.4 cm of seaward motion was measured by Interferometric Synthetic Aperture Radar (InSAR) satellite data (Froger et al., 2015). Since then, flank slip has slowed down and it is now taking place at a steady rate of 1.4 cm/year (Peltier et al., 2015). At this volcano, flank instability is mainly driven by magmatic activity (Poland et al., 2017), through intrusions in the main rift zones, and sheared intrusions along the subhorizontal part of a spoon-like structure connected to the rift-zone (Dumont et al., 2022; Tridon et al., 2016). Further along the structure, friction on a detachment surface (low angle normal fault) is resisting flank instability (Chaput et al., 2014).

Writing – original draft: A. Iozzia, G. Currenti, V. Cayol
Writing – review & editing: A. Iozzia, G. Currenti, V. Cayol, A. Bonforte, A. Cannata, J. L. Froger

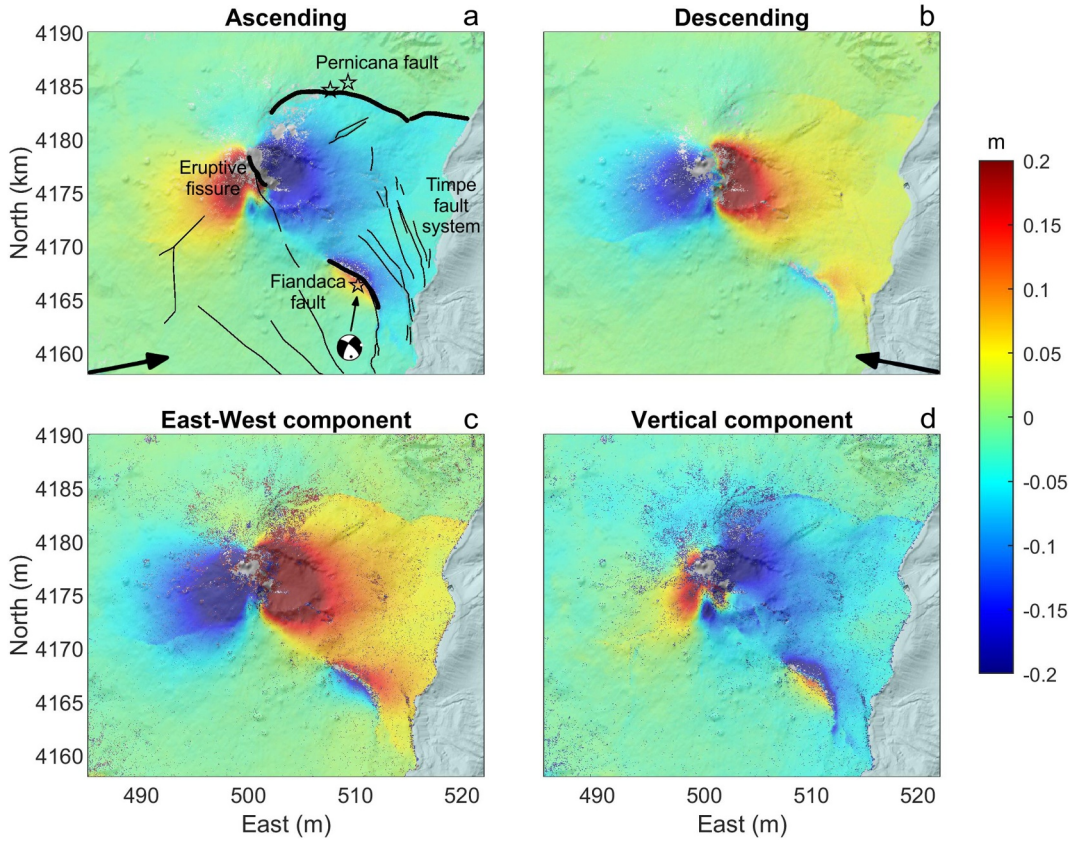

Figure 1. Ground displacement and main geological features at Etna. The data, acquired by the satellite Sentinel-1, cover the 22–28 December 2018 period, when an eruption took place. (a) Ascending and (b) descending LOS (line-of-sight of the satellite indicated by black arrows) displacements; (c) East-West displacement map and (d) vertical displacement map computed using the ascending and descending LOS data shown in (a, b). Black thick lines in (a) indicate the manually traced lines of the intrusion and the faults, while the thin lines represent the main Etna structural features known in literature (Barreca et al., 2013). The stars indicate the M3.2 and M3.5 Pernicana fault earthquakes recorded on 24 December 2018 and the M5.0 Fiandaca fault earthquake recorded on 26 December 2018 (focal mechanism from Alparone et al. (2020)). Coordinates are in the UTM grid system, zone 33N.

Mt. Etna bears several similarities with Piton de la Fournaise and Kilauea (Poland et al., 2017). Geological and geophysical observations indicate that flank slip of the eastern flank results from a complex interplay between magma intrusions, which often occurs along the rift-zones, gravitational spreading and tectonic forces that affect and slowly deform the basement of the volcano (Bonforte et al., 2008; Borgia et al., 1992; Gresta et al., 2005; Lundgren et al., 2004; Urlaub et al., 2018). Similarly to Piton de la Fournaise, flank slip is steadily taking place, but the rate is twice as large with values of at least 2–3 cm/yr (Bonforte et al., 2011). Similarly to Piton de la Fournaise and Kilauea, Etna's slip rates are sometimes accelerating after magmatic intrusions, reaching up 10 cm/yr, and exponentially decreasing for months to years (Alparone et al., 2013; Bonforte et al., 2007, 2013; Mattia et al., 2020; Ruch et al., 2013). The constant seaward motion, with higher velocities measured along the coastline, cannot be solely explained by magmatic sources on the central part of the volcano. When interpreting long term ground displacement, an additional source is often required, lying beneath and involving the eastern flank as a whole (Alparone et al., 2011; Bonaccorso et al., 2006; Bonforte & Puglisi, 2006). Inverse modeling of long-term ground deformation indicates that slip of the mobile sector is accommodated by an eastward dipping detachment (i.e., a low angle normal fault) located between sea level and 2 km b.s.l. beneath the summit region. The mobile sector is dissected by a number of faults, dividing the whole sector in many blocks (Azzaro et al., 2013; Barreca et al., 2013; Bonforte et al., 2011; Bonforte & Puglisi, 2006). To the north, it is limited by the Pernicana fault, which is characterized by creeping and seismogenic segments (Azzaro et al., 1998; Bonforte et al., 2007; Neri et al., 2004) and to the south by the Timpe fault system, which is formed by several segments among which the Fiandaca fault (Figure 1). From a seismotectonic point of view, these segments are very active both in terms of

number of earthquakes and magnitudes (Azzaro et al., 2017), even if many of them behave in a complex way with a wide spectrum of kinematics from stick-slip to slow slip (Azzaro et al., 2020).

A clear evidence of the complex interaction between magmatic and flank motion at Etna is provided by the eruption on 24 December 2018, later called the Christmas Eve eruption. The event, characterized by both explosive and effusive activity, lasted for a few days till lava emission stopped on 27 December 2018 (Calvari et al., 2020). Despite the relatively short duration and the limited emitted volume ($\sim 1 \times 10^6$ m^3; Bonforte et al., 2019; Cannavò et al., 2019; Laiolo et al., 2019), the intrusive phase caused an intense seismic crisis with more than 500 $M > 1$ events from 22 to 28 December (Alparone et al., 2022) and a strong ground deformation, reaching 60 cm in the summit area. The eruption caused a sudden acceleration of the eastern flank of the volcano (Mattia et al., 2020; Pezzo et al., 2023). Concurrently with the onset of the eruption, on 24 December, two earthquakes, with magnitudes of 3.2 and 3.5, occurred along the Pernicana fault (Figure 1) and two days later, on 26 December, at 02:19 UTC a M5.0 earthquake (revised magnitude from CPTI15 catalog; Rovida et al., 2021) struck the Fiandaca fault (Alparone et al., 2020; Giampiccolo et al., 2020).

By using GNSS and InSAR data, several studies have addressed the understanding of both the magma propagation and the flank slip response. Preliminary inversions, based on the Okada analytical model (Okada, 1985), considered two dykes and fault planes with homogeneous displacements (Bonforte et al., 2019). Other studies, in order to better explain the observed displacement, inverted for dykes and faults discretized into patches (Aloisi et al., 2020; Cannavò et al., 2019; De Novellis et al., 2019; Mattia et al., 2020). None of these studies considered the possibility of having curved fractures and faults and none fully considered the stress interactions between deformation sources. Some studies (De Novellis et al., 2019; Pezzo et al., 2020) computed Coulomb stress changes, showing that the intrusion had favored slip on the flank faults that failed during the eruption. A key question, unanswered so far, is whether the amount of slip on the flank faults was solely induced by the main intrusion, or whether it resulted from stress accumulation from previous intrusions and previous slip events on neighboring flank faults. Answering these questions will inform on the frictional behavior of the flank faults. Do they creep and passively respond to the summit intrusion or do they correspond to asperities and accumulate stress until they fail?

Our study addresses the mechanical understanding of the observed InSAR displacement. We rely on a 3D boundary element method (Cayol & Cornet, 1997) combined with inversions (Fukushima et al., 2005) to determine the volume and displacement accommodated by the intruded magma. We next analyze how stress changes, transmitted by intrusions to faults, trigger flank displacement. We invert for curved fractures and co-eval normal and shear stress change. Boundary element methods inherently consider stress interactions between sources, enabling us to determine the slip amount of flank faults directly triggered by the main intrusion.

2. Data and Methods

We study the ground displacements of the Christmas Eve eruption using both the ascending and descending interferograms acquired from the Sentinel-1 satellite. The satellite has a repeat time of 6 days, and, for both interferograms, we use the 22–28 December 2018 pair (Table S1 in Supporting Information S1) that spans the eruption. To convert the interferograms in line-of-sight (LOS) displacement, a recursive unwrapping method is used (Fukushima et al., 2005). To gain insight into the deformation sources, LOS displacement is decomposed into eastern and vertical displacement (Figure 1) using the approach of Wright et al. (2004). The displacement pattern is consistent with a dyke opening in the summit area and motions along the faults bordering the eastern flank. The eastern flank is undergoing subsidence and eastern displacement, while the western flank is experiencing uplift and western displacement. At the level of the Pernicana fault, sinistral displacement reaches 0.05 m on the western part of the fault and decreases to 0.01 m on the eastern part. The highest flank displacement takes place along the Fiandaca fault and reaches 0.3 m of dextral displacement.

Satellite observations are analyzed to constrain the magmatic intrusion and quantify the origin of slip along the faults using forward models combined with near-neighbor inversions (Fukushima et al., 2005). The forward modeling approach relies on a 3D Mixed Boundary Element Method (MBEM, Cayol & Cornet, 1997), which assumes linear elasticity, homogeneity, and isotropy of the medium. A Young's modulus of 5 GPa and a Poisson's ratio of 0.25 are considered, corresponding to in-situ measurements of Heap et al. (2020) on basaltic rock samples at Etna. Topography is taken into account, as neglecting it may lead to errors in the estimation of intrusion depths and volume changes (Cayol & Cornet, 1998; Currenti, Del Negro, Ganci, & Scandura, 2008; Fukushima

et al., 2005; Trasatti et al., 2007). Before starting any computation, the topography mesh providing the best compromise between precision and efficiency is determined (Figures S1 and S2 in Supporting Information S1). Boundaries, representing the topography, fractures, and faults, are meshed by triangular elements. Boundary conditions are defined in terms of stresses. At the ground surface, stress-free conditions are imposed. On the source surfaces, stress is assigned as homogeneous pressure and shear stress changes. When faults are assumed to respond passively, no stress changes are imposed in the model, which means that the faults move in response to the stress induced by the active sources. Buried dykes (i.e., dykes not reaching the ground surface) are described by 8 geometrical parameters (Figure S3 in Supporting Information S1), while sheared intrusions and faults connected to the ground are described by 9 (including along dip and along strike curvatures) and 4 geometrical parameters, respectively (Figure S4 in Supporting Information S1). Their rake is also considered. The realistic surface expression of these fractures is derived from SAR data or field mapping. Indeed, the high spatial resolution of the SAR data allows to constrain the traces of the eruptive fissure and of the faults at the ground surface, whose complex shapes are described as curves. Eruptive fissure location and orientation are defined using the COSMO-SkyMed ascending SAR amplitude image of 30 December (De Novellis et al., 2019), whereas the Pernicana and the Fiandaca faults traces are defined using the sharp displacement discontinuities visible in the Sentinel-1 data (Figure 1). These discontinuities are in good agreement with field mapping of surface ruptures (Azzaro et al., 2022).

Since displacement is a non-linear function of the geometrical parameters and of the rake, and a linear function of the stress changes, the geometrical parameters and the rake are inverted using a Monte Carlo neighborhood inversion (Fukushima et al., 2005), while the homogeneous pressure and shear stress changes are linearly inverted following Tridon et al. (2016). The neighborhood inversion consists of two stages, a search stage and an appraisal stage (Sambridge, 1999a, 1999b). In the search stage (Sambridge, 1999a), the model parameters that best explain the observed data are searched for iteratively in the vicinity of previously determined best-fit models, where the vicinity of models in the parameters space is defined by voronoï cells. A misfit function $\%\chi^2 = (d_{\text{obs}} - d_m)^T C_d^{-1} (d_{\text{obs}} - d_m)$, is minimized, where d_{obs} is the observed displacement, d_m is the modeled displacement and C_d is the full covariance matrix, that considers the data noise is exponentially correlated (see Fukushima et al., 2005). To make the computation of C_d^{-1} numerically manageable, while keeping relevant information, both the ascending and descending data are subsampled, using an adaptive quadtree decomposition algorithm (Jónsson et al., 2002; Welstead, 1999), leading to approximately 500 points per track (Table S1 in Supporting Information S1). To determine the best compromise between the data fit and the model complexity, following Fukushima et al. (2010), we use the Akaike Information Criteria (AIC, Akaike, 1974). From a statistical point of view, the lower the AIC, the better the model. The appraisal stage (Sambridge, 1999b) concerns the evaluation of the model uncertainties (confidence intervals and mean model parameters). Relying on a Bayesian inference, models computed in the search stage are resampled, enabling the computation of posterior probability density functions from models computed in the search stage.

3. Results

The summit displacement pattern and the summit fissures are a few kilometers away from the Pernicana and Fiandaca faults. Consequently, we assume that these faults have a negligible influence on the summit fissure, and hence we start analyzing the summit area separately from the flank faults. Moreover, since the deformation related to the detachment surface has mid- to long-term effects (Bonforte et al., 2019), it is considered negligible in the short analyzed period (22–28 December) and it is not taken into account in the modeling.

We investigate several models that could explain the summit displacement. Among them, we explore whether a dyke (Figure S5 in Supporting Information S1) or a sheared intrusion (Figure S6 in Supporting Information S1), reaching the surface at the location of the eruptive fissure and feeding the eruption, could explain the subsidence and the large extent of lateral displacements of the volcano's eastern flank. A simple dyke leads to a root mean square (RMS) error of 5.2 cm, while a sheared intrusion reduces the RMS error to 4.8 cm (Table S2 in Supporting Information S1), better explaining the eastern flank displacement. The AIC associated with the sheared intrusion is also smaller than for the simple dyke (1593 against 2356), indicating that a sheared intrusion is more likely. Because the sheared intrusion is too shallow to be consistent with earthquake hypocenters (Alparone et al., 2020), we decide to investigate the benefit of adding a buried dyke. The RMS error is further reduced reaching 2.5 cm

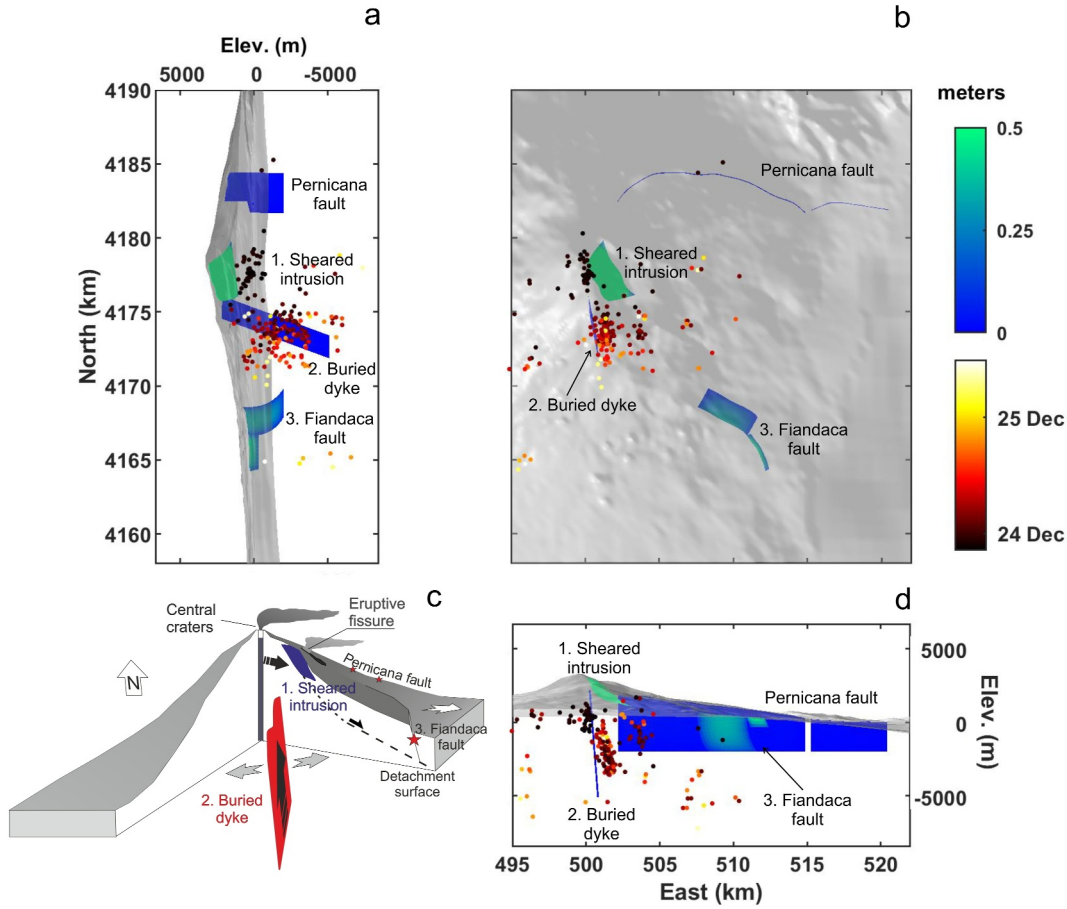

Figure 2. Source geometries and shear displacement of the best-fit model. (a) N-S view; (b) Map view; (c) Summary sketch; (d) E-W view. This model consists of a sheared intrusion, a buried dyke, and Pernicana and Fiandaca faults. Pernicana is passively responding, whereas Fiandaca is submitted to a shear stress drop. The colors of the sources indicate the shear displacement amplitudes. The dots indicate the earthquakes recorded by the Istituto Nazionale di Geofisica e Vulcanologia - Osservatorio Etneo (INGV-OE) on the 24 and 25 December 2018. The colors of the dots indicate the time of occurrence of the earthquakes. The numbers show the sequence of the events (1. Sheared intrusion; 2. Buried dyke; 3. Fiandaca fault rupture). The summary sketch depicts the possible link between the detachment surface (dashed line), the sheared intrusion, and the Fiandaca fault.

and the AIC (Table S2 in Supporting Information S1) is divided by three (550). Hence, this two source model provides the best-fit for the eruptive phase (Figure S7 in Supporting Information S1).

The sheared intrusion undergoes more slip than opening, with an average slip of about 1.3 m and an average opening of about 0.2 m. The maximum slip reaches 2.5 m and the maximum opening is 1.1 m. The corresponding volume change is 1.6×10^6 m^3. This intrusion is shallow, extending from the ground surface to 2500 m above sea level (a.s.l) for a mean elevation of ∼1300 m a.s.l (Figure 2, Table S3 and Figure S8 in Supporting Information S1). The intrusion has a dip of 40° and a vertical curvature of 23°. The buried dyke, which is only submitted to a pressure change, mainly undergoes an opening with an average value of about 1.8 m for an average slip of about 0.02 m. The small slip of the dyke is a consequence of the interaction of the dyke with the sheared intrusion, which is located 300 m above the dyke. The 8 km high dyke extends from ∼2200 m a.s.l down to 5800 m below sea level (b.s.l.) (Figure 2, Table S4 and Figure S9 in Supporting Information S1). This source is almost vertical and the orientation is approximately N-S. The volume change is 1.9×10^7 m^3, nearly 10 times as large as the volume change of the sheared intrusion.

To estimate the stress transferred by both magmatic intrusions to the flank faults, we compute the Coulomb stress changes (ΔCFF) induced on the Pernicana and the Fiandaca faults. Since the Pernicana fault mostly shows sinistral strike-slip, for simplicity, it is approximated as a vertical structure with a constant depth (fixed to 2 km b.

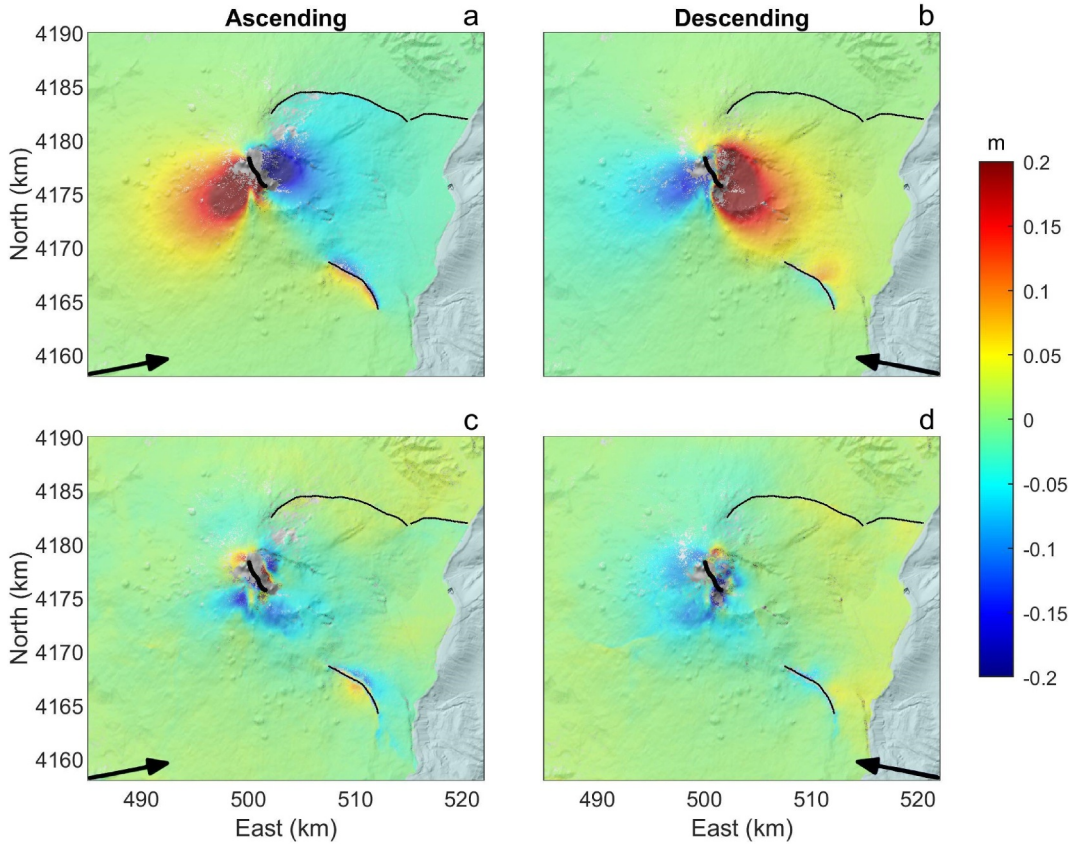

Figure 3. Displacement and residuals of the best-fit model. Ascending (a) and descending (b) modeled displacements, and ascending (c) and descending (d) residuals for the model using a sheared intrusion and a buried dyke, in which the 2 segments of the Fiandaca fault have an added shear stress drop, while the Pernicana fault is free to slip, without adding a stress drop.

s.l.), despite subtle variations of the dip along its strike (Azzaro et al., 2012, 2013; Barreca et al., 2013); also the dextral Fiandaca fault is approximated as a 2 km b.s.l. deep vertical fault (Azzaro et al., 2012, 2013; Barreca et al., 2013). Coulomb stress computation induced by each individual intrusion is needed to estimate the respective contribution of the sheared intrusion (mainly shear stress) and the deep intrusion (mainly normal stress). We find that, despite its shallower location and its more moderate volume, the sheared intrusion contributes twice as much to the enhancement of the ΔCFF on the Pernicana fault (Figure S10 in Supporting Information S1). Moreover, from induced displacements, we infer that strain is maximum where the strike of the Pernicana fault changes direction. On the contrary, the buried dyke induces a higher ΔCFF on the Fiandaca fault than the sheared intrusion (Figure S11 in Supporting Information S1).

To address the frictional behavior of the faults that limit the eastern flank, we investigate whether they passively respond to the stress changes due to the main intrusions. We find that stress changes induced by the main intrusions are sufficient to induce an amount of slip on the Pernicana fault consistent with the observations (Figure S12 in Supporting Information S1). The pattern of shear displacement on the Pernicana fault surface indicates a stress accumulation related to the change in the along-strike direction (Figure S13 in Supporting Information S1). However, differently from the Pernicana fault, the stress transferred by the summit area intrusions is not sufficient to induce displacements as large as those observed in the Fiandaca fault. Consequently, we consider this fault independently. Rather than assuming Fiandaca fault freely responds to the main intrusions, we assume stress had been accumulating, probably since the previous seismic event in 1984, and we invert for the amount of stress that was released in 2018. The Fiandaca fault is split into two segments in agreement with the two principal displacement zones identified during field mapping (Azzaro et al., 2022). For both segments, dips, bottom elevations, vertical curvatures, rakes, and shear stress drops are inverted (Table S5 in Supporting Information S1), relaxing the hypothesis of a constant depth made for ΔCFF computation. The best-fit fault model (Figure 2),

according to the RMS error and AIC, corresponds to a 2 km b.s.l. deep curved fault segment to the North and a shallower planar fault segment to the South. Highest residuals (Figure 3c, 3d) affect the summit part of the volcano, imputable to the near-field non-elastic deformation close to the sheared intrusion and to the geometrical simplification of the fracture surface, inherent to any modeling procedure. A couple of centimeters remain unexplained on the eastern side of Etna. They could be related to some slip on the detachment. Slip on the northern Fiandaca segment has an average value of 0.22 m, while that on the southern Fiandaca segment has an average value of 0.31 m, consistent with a maximum eastward slip of 0.2 m at the faults level. Slip of the northern segment has a rake of 163°, suggesting an almost purely right-lateral strike-slip movement, while slip of the southern segment has a rake of 135°, suggesting a larger normal component, characteristic of a transtensive right-lateral movement (Table S5 in Supporting Information S1).

4. Discussion and Conclusions

Using a consistent mechanical model and high spatial resolution SAR data, we quantitatively explored the interaction between magmatic and tectonic processes during the Christmas Eve eruption at Etna in 2018. Our model explains the summit displacement associated with the eruption by the interaction between two intrusion sources, a buried dyke and a curved sheared intrusion, reaching the surface and feeding the eruption. Similarly to previous studies, we determine that several sources are needed. However, our results differ in terms of mechanism (slip and opening) and geometries of the two sources. Previous studies used simple Okada sources, while we used sources with complex geometries, demonstrating the role of curved sheared intrusion in the shallower area of the volcano. Bonforte et al. (2019) found a model composed of two dykes, one shallow and one deep, and a deflation source. Both dykes show values of opening similar to each other (~1 m), while, in our model, the buried dyke has a higher opening (1.8 m) that generates a volume change of 19×10^6 m^3 over a smaller surface. The extent of the dyke surface better fits the earthquake pattern. De Novellis et al. (2019) determined two planar opening dykes, one to the North, 4 km deep, and the other to the south, 8 km deep similar to ours, but more than twice longer. Our findings show an important contribution from the sheared intrusion. Using a simple tensile opening mechanism for this intrusion the model is not capable of explaining the larger subsidence of the eastern flank of the volcano, and an additional deflating source is needed, as in Bonforte et al. (2019). On the contrary, a sheared intrusion provides the best solution for the observed displacement. Sheared intrusions typically take place when magma is guided by a preexisting discontinuity, in which case magma is not necessarily emplaced perpendicular to the minimum principal stress and consequently relaxes the shear stress acting on the discontinuity (Cayol et al., 2014; Chaput et al., 2014; Delaney et al., 1986). The role of sheared intrusions in volcanoes showing flank instabilities has been reported by geological studies at the Piton des Neiges volcano, Reunion Island (Berthod et al., 2016; Famin & Michon, 2010) and from an extensive InSAR study at Piton de la Fournaise volcano (Dumont et al., 2022). At this volcano, buried sheared intrusions take place in the subhorizontal part of a flank slip structure away from the summit. However, at Etna during the Christmas Eve eruption, in contrast with Piton de la Fournaise, lateral displacement took place close to the summit, in a location that may be the head of the flank slip structure identified by previous studies (Bonforte & Puglisi, 2006; Bonforte et al., 2013; Siniscalchi et al., 2012).

The location of both sources is consistent with the observed volcano-tectonic earthquakes that occurred before and during the eruption (Figure 2). Both intrusions are determined to be separated in space, similarly to the seismicity patterns accompanying their propagations (Figure 2). The temporal distribution of the seismicity indicates an initial shallow swarm (from 1 km b.s.l. to 2 km a.s.l.) related to the sheared intrusion, followed by a deep swarm (from 6 km b.s.l.) associated with the buried dyke (Alparone et al., 2020). A likely scenario is that the buried dyke is guided from depth toward the surface by one of the main weakness zones associated with the South Rift. As already observed during the 2001 and 2002–2003 eruptions at Etna (Currenti, Del Negro, Ganci, & Williams, 2008; Gresta et al., 2005; Monaco et al., 2005), it is plausible that magma feeding the two intrusions came from two different plumbing systems. The magma supplying the summit eruptive fissures, transmitted by the sheared intrusion, could have departed from a very shallow portion of the magmatic system or from the central conduit (Figure 2c). Whereas the magma intruded into the buried dyke could be supplied by an independent deeper reservoir as already observed in the above mentioned lateral eruptions at Etna. The simultaneous involvement of distinct magmas in previous eruptive activities has been proven by petrologic analysis of the erupted products (Monaco et al., 2005). For the Christmas Eve eruption, the deeper dyke being arrested at depth, we cannot definitively prove this hypothesis.

Before, during and after the eruption, the volcano's eastern flank was characterized by an increase in seismicity and, as indicated by the InSAR data, the whole flank underwent an accelerated eastward displacement, along a sector bounded by the Pernicana and the Fiandaca faults. We find that stress induced by the summit intrusions triggered the observed slip on the Pernicana fault. In particular, similarly to a previous study (Currenti et al., 2012), we infer that strain was maximum at a location where the fault changes direction. This strain accumulation coincides with the location of the two main seismic events which took place along the Pernicana fault (Figure S12 in Supporting Information S1). This area corresponds to a fault portion characterized by the highest generation of repeating earthquakes in the entire Pernicana fault (Cannata et al., 2021). Along the Fiandaca fault, on the contrary, stress of the main intrusions is not large enough to promote the observed fault movement. This implies that the Fiandaca fault has been accumulating stress, probably since its last seismic event (Azzaro et al., 2017). The two fault segments used to model the displacement of the Fiandaca fault show different values of dip, curvature, and depth. In particular, the northern segment is found to be curved along its dip, demonstrating for the first time at Etna the existence of a listric fault as suggested by Azzaro et al. (2013). The depth of the bottom part of the fault (2 km b.s.l.) is consistent with the depth of the detachment surface (from 2 to 4 km b.s.l.; Bonforte & Puglisi, 2003), inferred from the inversion of long-term ground deformation. This suggests that the obtained listric fault may join the detachment surface at depth. The curvature determined is a robust result. Indeed, when trying to explain displacements associated with the Fiandaca fault, with 2–4 planar segments, an unrealistically deep middle segment (up to 8 km b.s.l.) is needed in order to explain the amount of displacement to the North-East. On the other hand, the southern segment determined is almost vertical, planar, and shallower. It accommodates a small amount of transtensive motion, consistent with field studies conducted soon after the 2018 events (Azzaro et al., 2022). Overall all the faults show a displacement consistent with the east-southeast flank motion: when the fault is parallel to the flank motion, slip is right lateral; when it is perpendicular to the flank motion, it is transtensive. Note that most observed flank displacement can be explained disregarding the contribution of the detachment slip. It may have taken place, but its influence is secondary in such a short period.

Our numerical models demonstrate the complex interplay between the magmatic activity and the fault response on the eastern flank at Etna, which would have been difficult to explain with simple model assumptions. The accurate definition of fault and fissure traces, the use of curved surfaces, the inversion of stress changes, whether normal or sheared, and consideration of interacting sources, led to fit the observed InSAR displacement with a more reduced number of unknowns than when considering opening and slip distributions over patches. Most importantly, these numerical models allowed us to investigate the flank fault response under different conditions (passively responding or not) avoiding artifacts generated by simple dislocation models. The use of mechanically consistent models for the interpretation of dense spatial ground deformation helps improve the determination of the geometry and the response of the fault system at depth and unravels their interaction with the magmatic system.

Data Availability Statement

Ascending and descending LOS displacements are available from Iozzia et al. (2024). Inverse models were conducted using the DefVolc software, which is available online (http://opgc.fr/defvolc).

Acknowledgments

A.I. thanks the IMPACT project—"A multidisciplinary Insight on the kinematics and dynamics of Magmatic Processes at Mt. Etna Aimed at identifying preCursor phenomena and developing early warning sysTems," funded by INGV-Progetto Strategico Dipartimento Vulcani 2019 (Delibera n. 144/2020). This is Laboratory of Excellence ClerVolc contribution number 646. Inversions have been performed on the supercomputer facilities of the Mésocentre Clermont-Auvergne.

References

Akaike, H. (1974). A new look at the statistical model identification. *IEEE Transactions on Automatic Control*, *19*(6), 716–723. https://doi.org/10.1109/TAC.1974.1100705

Aloisi, M., Bonaccorso, A., Cannavò, F., Currenti, G., & Gambino, S. (2020). The 24 December 2018 eruptive intrusion at Etna volcano as revealed by multidisciplinary continuous deformation networks (CGPS, borehole strainmeters and tiltmeters). *Journal of Geophysical Research: Solid Earth*, *125*(8), e2019JB019117. https://doi.org/10.1029/2019JB019117

Alparone, S., Barberi, G., Bonforte, A., Maiolino, V., & Ursino, A. (2011). Evidence of multiple strain fields beneath the eastern flank of Mt. Etna volcano (Sicily, Italy) deduced from seismic and geodetic data during 2003–2004. *Bulletin of Volcanology*, *73*(7), 869–885. https://doi.org/10.1007/s00445-011-0456-1

Alparone, S., Barberi, G., Di Grazia, G., Giampiccolo, E., Maiolino, V., Mostaccio, A., et al. (2022). Mt. Etna seismic catalog 2017–2019 (version 1) [Dataset]. *Istituto Nazionale di Geofisica e Vulcanologia (INGV)*. https://doi.org/10.13127/ETNASC/2017_2019

Alparone, S., Barberi, G., Giampiccolo, E., Maiolino, V., Mostaccio, A., Musumeci, C., et al. (2020). Seismological constraints on the 2018 Mt. Etna (Italy) flank eruption and implications for the flank dynamics of the volcano. *Terra Nova*, *32*(5), 334–344. https://doi.org/10.1111/ter.12463

Alparone, S., Bonaccorso, A., Bonforte, A., & Currenti, G. (2013). Long-term stress-strain analysis of volcano flank instability: The eastern sector of Etna from 1980 to 2012. *Journal of Geophysical Research: Solid Earth*, *118*(9), 5098–5108. https://doi.org/10.1002/jgrb.50364

Auker, M. R., Sparks, R. S. J., Siebert, L., Crosweller, H. S., & Ewert, J. (2013). A statistical analysis of the global historical volcanic fatalities record. *Journal of Applied Volcanology*, *2*, 1–24. https://doi.org/10.1186/2191-5040-2-2

Azzaro, R., Barberi, G., D'Amico, S., Pace, B., Peruzza, L., & Tuvè, T. (2017). When probabilistic seismic hazard climbs volcanoes: The Mt. Etna case, Italy–Part 1: Model components for sources parameterization. *Natural Hazards and Earth System Sciences*, *17*(11), 1981–1998. https://doi.org/10.5194/nhess-17-1981-2017

Azzaro, R., Bonforte, A., Branca, S., & Guglielmino, F. (2013). Geometry and kinematics of the fault systems controlling the unstable flank of Etna volcano (Sicily). *Journal of Volcanology and Geothermal Research*, *251*, 5–15. https://doi.org/10.1016/j.jvolgeores.2012.10.001

Azzaro, R., Bonforte, A., D'Amico, S., Guglielmino, F., & Scarfì, L. (2020). Stick-slip vs. stable sliding fault behaviour: A case-study using a multidisciplinary approach in the volcanic region of Mt. Etna (Italy). *Tectonophysics*, *790*, 228554. https://doi.org/10.1016/j.tecto.2020.228554

Azzaro, R., Branca, S., Giammanco, S., Gurrieri, S., Rasà, R., & Valenza, M. (1998). New evidence for the form and extent of the Pernicana Fault System (Mt. Etna) from structural and soil–gas surveying. *Journal of Volcanology and Geothermal Research*, *84*(1–2), 143–152. https://doi.org/10.1016/S0377-0273(98)00036-5

Azzaro, R., Branca, S., Gwinner, K., & Coltelli, M. (2012). The volcano-tectonic map of Etna volcano, 1: 100.000 scale: An integrated approach based on a morphotectonic analysis from high-resolution DEM constrained by geologic, active faulting and seismotectonic data. *Italian Journal of Geosciences*, *131*(1), 153–170. https://doi.org/10.3301/IJG.2011.29

Azzaro, R., Pucci, S., Villani, F., Civico, R., Branca, S., Cantarero, M., et al. (2022). Surface faulting of the 26 December 2018, Mw5 earthquake at Mt. Etna volcano (Italy): Geological source model and implications for the seismic potential of the Fiandaca fault. *Tectonics*, *41*(12), e2021TC007182. https://doi.org/10.1029/2021TC007182

Barreca, G., Bonforte, A., & Neri, M. (2013). A pilot GIS database of active faults of Mt. Etna (Sicily): A tool for integrated hazard evaluation. *Journal of Volcanology and Geothermal Research*, *251*, 170–186. https://doi.org/10.1016/j.jvolgeores.2012.08.013

Berthod, C., Famin, V., Bascou, J., Michon, L., Ildefonse, B., & Monie, P. (2016). Evidence of sheared sills related to flank destabilization in a basaltic volcano. *Tectonophysics*, *674*, 195–209. https://doi.org/10.1016/j.tecto.2016.02.017

Bonaccorso, A., Bonforte, A., Guglielmino, F., Palano, M., & Puglisi, G. (2006). Composite ground deformation pattern forerunning the 2004–2005 Mount Etna eruption. *Journal of Geophysical Research*, *111*(B12), B12207. https://doi.org/10.1029/2005JB004206

Bonforte, A., Bonaccorso, A., Guglielmino, F., Palano, M., & Puglisi, G. (2008). Feeding system and magma storage beneath Mt. Etna as revealed by recent inflation/deflation cycles. *Journal of Geophysical Research*, *113*(5), B05406. https://doi.org/10.1029/2007JB005334

Bonforte, A., Branca, S., & Palano, M. (2007). Geometric and kinematic variations along the active Pernicana fault: Implication for the dynamics of Mount Etna NE flank (Italy). *Journal of Volcanology and Geothermal Research*, *160*(1–2), 210–222. https://doi.org/10.1016/j.jvolgeores.2006.08.009

Bonforte, A., Guglielmino, F., Coltelli, M., Ferretti, A., & Puglisi, G. (2011). Structural assessment of Mount Etna volcano from Permanent Scatterers analysis. *Geochemistry, Geophysics, Geosystems*, *12*(2), Q02002. https://doi.org/10.1029/2010GC003213

Bonforte, A., Guglielmino, F., & Puglisi, G. (2013). Interaction between magma intrusion and flank dynamics at Mt. Etna in 2008, imaged by integrated dense GPS and DInSAR data. *Geochemistry, Geophysics, Geosystems*, *14*(8), 2818–2835. https://doi.org/10.1002/ggge.20190

Bonforte, A., Guglielmino, F., & Puglisi, G. (2019). Large dyke intrusion and small eruption: The December 24, 2018 Mt. Etna eruption imaged by Sentinel-1 data. *Terra Nova*, *31*(4), 405–412. https://doi.org/10.1111/ter.12403

Bonforte, A., & Puglisi, G. (2003). Magma uprising and flank dynamics on Mount Etna volcano, studied using GPS data (1994–1995). *Journal of Geophysical Research*, *108*(B3), 2153. https://doi.org/10.1029/2002JB001845

Bonforte, A., & Puglisi, G. (2006). Dynamics of the eastern flank of Mt. Etna volcano (Italy) investigated by a dense GPS network. *Journal of Volcanology and Geothermal Research*, *153*(3–4), 357–369. https://doi.org/10.1016/j.jvolgeores.2005.12.005

Borgia, A., Ferrari, L., & Pasquarè, G. (1992). Importance of gravitational spreading in the tectonic and volcanic evolution of Mount Etna. *Nature*, *357*(6375), 231–235. https://doi.org/10.1038/357231a0

Butler, R. (2019). Composite earthquake source mechanism for 2018 Mw 5.2–5.4 swarm at Kīlauea Caldera: Antipodal source constraint. *Seismological Research Letters*, *90*(2A), 633–641. https://doi.org/10.1785/0220180288

Calvari, S., Bilotta, G., Bonaccorso, A., Caltabiano, T., Cappello, A., Corradino, C., et al. (2020). The VEI 2 Christmas 2018 Etna eruption: A small but intense eruptive event or the starting phase of a larger one? *Remote Sensing*, *12*(6), 905. https://doi.org/10.3390/rs12060905

Cannata, A., Iozzia, A., Alparone, S., Bonforte, A., Cannavò, F., Cesca, S., et al. (2021). Repeating earthquakes and ground deformation reveal the structure and triggering mechanisms of the Pernicana fault, Mt. Etna. *Communications Earth and Environment*, *2*(1), 116. https://doi.org/10.1038/s43247-021-00188-6

Cannavò, F., Sciotto, M., Cannata, A., & Di Grazia, G. (2019). An integrated geophysical approach to track magma intrusion: The 2018 Christmas Eve eruption at Mount Etna. *Geophysical Research Letters*, *46*(14), 8009–8017. https://doi.org/10.1029/2019GL083120

Cayol, V., Catry, T., Michon, L., Chaput, M., Famin, V., Bodart, O., et al. (2014). Sheared sheet intrusions as mechanism for lateral flank displacement on basaltic volcanoes: Applications to Réunion Island volcanoes. *Journal of Geophysical Research: Solid Earth*, *119*(10), 7607–7635. https://doi.org/10.1002/2014JB011139

Cayol, V., & Cornet, F. H. (1997). 3D mixed boundary elements for elastostatic deformation field analysis. *International Journal of Rock Mechanics and Mining Sciences*, *34*(2), 275–287. https://doi.org/10.1016/S0148-9062(96)00035-6

Cayol, V., & Cornet, F. H. (1998). Effects of topography on the interpretation of the deformation field of prominent volcanoes—Application to Etna. *Geophysical Research Letters*, *25*(11), 1979–1982. https://doi.org/10.1029/98GL51512

Cayol, V., Dieterich, J. H., Okamura, A. T., & Miklius, A. (2000). High magma storage rates before the 1983 eruption of Kilauea, Hawaii. *Science*, *288*(5475), 2343–2346. https://doi.org/10.1126/science.288.5475.2343

Chaput, M., Pinel, V., Famin, V., Michon, L., & Froger, J. L. (2014). Co-Intrusive shear displacement by sill intrusion in a detachment: A numerical approach. *Geophysical Research Letters*, *41*(6), 1937–1943. https://doi.org/10.1002/2013GL058813

Currenti, G., Del Negro, C., Ganci, G., & Scandura, D. (2008). 3D numerical deformation model of the intrusive event forerunning the 2001 Etna eruption. *Physics of the Earth and Planetary Interiors*, *168*(1–2), 88–96. https://doi.org/10.1016/j.pepi.2008.05.004

Currenti, G., Del Negro, C., Ganci, G., & Williams, C. (2008). Static stress changes induced by the magmatic intrusions during the 2002-2003 Etna eruption. *Journal of Geophysical Research*, *113*(B10), B10206. https://doi.org/10.1029/2007JB005301

Currenti, G., Solaro, G., Napoli, R., Pepe, A., Bonaccorso, A., Del Negro, C., & Sansosti, E. (2012). Modeling of ALOS and COSMO-SkyMed satellite data at Mt Etna: Implications on relation between seismic activation of the Pernicana fault system and volcanic unrest. *Remote Sensing of Environment*, *125*, 64–72. https://doi.org/10.1016/j.rse.2012.07.008

Delaney, P. T., Pollard, D. D., Ziony, J. I., & McKee, E. H. (1986). Field relations between dikes and joints: Emplacement processes and paleostress analysis. *Journal of Geophysical Research*, *91*(B5), 4920–4938. https://doi.org/10.1029/JB091iB05p04920

Denlinger, R. P., & Morgan, J. K. (2014). Instability of Hawaiian volcanoes. *Characteristics of Hawaiian Volcanoes*, *1801*, 149–176. https://doi.org/10.3133/pp18014

De Novellis, V., Atzori, S., De Luca, C., Manzo, M., Valerio, E., Bonano, M., et al. (2019). DInSAR analysis and analytical modeling of Mount Etna displacements: The December 2018 volcano-tectonic crisis. *Geophysical Research Letters*, *46*(11), 5817–5827. https://doi.org/10.1029/2019GL082467

Dieterich, J. H. (1988). Growth and persistence of Hawaiian volcanic rift zones. *Journal of Geophysical Research*, *93*(B5), 4258–4270. https://doi.org/10.1029/JB093iB05p04258

Dumont, Q., Cayol, V., Froger, J. L., & Peltier, A. (2022). 22 years of satellite imagery reveal a major destabilization structure at Piton de la Fournaise. *Nature Communications*, *13*(1), 2649. https://doi.org/10.1038/s41467-022-30109-w

Famin, V., & Michon, L. (2010). Volcano destabilization by magma injections in a detachment. *Geology*, *38*(3), 219–222. https://doi.org/10.1130/G30717.1

Froger, J. L., Famin, V., Cayol, V., Augier, A., Michon, L., & Lénat, J. F. (2015). Time-dependent displacements during and after the April 2007 eruption of Piton de la Fournaise, revealed by interferometric data. *Journal of Volcanology and Geothermal Research*, *296*, 55–68. https://doi.org/10.1016/j.jvolgeores.2015.02.014

Fukushima, Y., Cayol, V., & Durand, P. (2005). Finding realistic dike models from interferometric synthetic aperture radar data: The February 2000 eruption at Piton de la Fournaise. *Journal of Geophysical Research*, *110*(B3), B03206. https://doi.org/10.1029/2004JB003268

Fukushima, Y., Cayol, V., Durand, P., & Massonnet, D. (2010). Evolution of magma conduits during the 1998–2000 eruptions of Piton de la Fournaise volcano, Réunion Island. *Journal of Geophysical Research*, *115*(B10), B10204. https://doi.org/10.1029/2009JB007023

Giampiccolo, E., Cocina, O., De Gori, P., & Chiarabba, C. (2020). Dyke intrusion and stress-induced collapse of volcano flanks: The example of the 2018 event at Mt. Etna (Sicily, Italy). *Scientific Reports*, *10*(1), 6373. https://doi.org/10.1038/s41598-020-63371-3

Gresta, S., Ghisetti, F., Privitera, E., & Bonanno, A. (2005). Coupling of eruptions and earthquakes at Mt. Etna (Sicily, Italy): A case study from the 1981 and 2001 events. *Geophysical Research Letters*, *32*(5), 1–4. https://doi.org/10.1029/2004GL021479

Heap, M. J., Villeneuve, M., Albino, F., Farquharson, J. I., Brothelande, E., Amelung, F., et al. (2020). Towards more realistic values of elastic moduli for volcano modelling. *Journal of Volcanology and Geothermal Research*, *390*, 106684. https://doi.org/10.1016/j.jvolgeores.2019.106684

Iozzia, A., Currenti, G., Cayol, V., Bonforte, A., Cannata, A., & Froger, J. L. (2024). Ascending and descending LOS displacements [Dataset]. *Figshare*. https://doi.org/10.6084/m9.figshare.25434817.v1

Iverson, R. M. (1995). Can magma-injection and groundwater forces cause massive landslides on Hawaiian volcanoes? *Journal of Volcanology and Geothermal Research*, *66*(1–4), 295–308. https://doi.org/10.1016/0377-0273(94)00064-N

Jónsson, S., Zebker, H., Segall, P., & Amelung, F. (2002). Fault slip distribution of the 1999 Mw 7.1 Hector Mine, California, earthquake, estimated from satellite radar and GPS measurements. *Bulletin of the Seismological Society of America*, *92*(4), 1377–1389. https://doi.org/10.1785/0120000922

Laiolo, M., Ripepe, M., Cigolini, C., Coppola, D., Della Schiava, M., Genco, R., et al. (2019). Space-and ground-based geophysical data tracking of magma migration in shallow feeding system of Mount Etna Volcano. *Remote Sensing*, *11*(10), 1182. https://doi.org/10.3390/rs11101182

Lundgren, P., Casu, F., Manzo, M., Pepe, A., Berardino, P., Sansosti, E., & Lanari, R. (2004). Gravity and magma induced spreading of Mount Etna volcano revealed by satellite radar interferometry. *Geophysical Research Letters*, *31*(4), L04602. https://doi.org/10.1029/2003GL018736

Mattia, M., Bruno, V., Montgomery-Brown, E., Patanè, D., Barberi, G., & Coltelli, M. (2020). Combined seismic and geodetic analysis before, during, and after the 2018 Mount Etna eruption. *Geochemistry, Geophysics, Geosystems*, *21*(9), e2020GC009218. https://doi.org/10.1029/2020GC009218

Miklius, A., Cervelli, P., Sako, M., Lisowski, M., Owen, S., Segal, P., et al. (2005). Global positioning system measurements on the Island of Hawai'i: 1997 through 2004. *US Geol. Surv. Open File Rep*, *1425*, 1–48.

Monaco, C., Catalano, S., Cocina, O., De Guidi, G., Ferlito, C., Gresta, S., et al. (2005). Tectonic control on the eruptive dynamics at Mt. Etna Volcano (Sicily) during the 2001 and 2002–2003 eruptions. *Journal of Volcanology and Geothermal Research*, *144*(1–4), 211–233. https://doi.org/10.1016/j.jvolgeores.2004.11.024

Montgomery-Brown, E. K., Poland, M. P., & Miklius, A. (2015). Delicate balance of magmatic-tectonic interaction at Kīlauea volcano, Hawai 'i, revealed from slow slip events. *Hawaiian Volcanoes: From Source to Surface*, 269–288. https://doi.org/10.1002/9781118872079.ch13

Neri, M., Acocella, V., & Behncke, B. (2004). The role of the Pernicana Fault System in the spreading of Mt. Etna (Italy) during the 2002–2003 eruption. *Bulletin of Volcanology*, *66*(5), 417–430. https://doi.org/10.1007/s00445-003-0322-x

Okada, Y. (1985). Surface deformation due to shear and tensile faults in a half-space. *Bulletin of the Seismological Society of America*, *75*(4), 1135–1154. https://doi.org/10.1785/BSSA0750041135

Owen, S. E., & Bürgmann, R. (2006). An increment of volcano collapse: Kinematics of the 1975 Kalapana, Hawaii, earthquake. *Journal of Volcanology and Geothermal Research*, *150*(1–3), 163–185. https://doi.org/10.1016/j.jvolgeores.2005.07.012

Peltier, A., Got, J. L., Villeneuve, N., Boissier, P., Staudacher, T., Ferrazzini, V., & Walpersdorf, A. (2015). Long-term mass transfer at Piton de la Fournaise volcano evidenced by strain distribution derived from GNSS network. *Journal of Geophysical Research: Solid Earth*, *120*(3), 1874–1889. https://doi.org/10.1002/2014JB011738

Pezzo, G., Palano, M., Beccaro, L., Tolomei, C., Albano, M., Atzori, S., & Chiarabba, C. (2023). Coupling flank collapse and magma dynamics on stratovolcanoes: The Mt. Etna example from InSAR and GNSS observations. *Remote Sensing*, *15*(3), 847. https://doi.org/10.3390/rs15030847

Pezzo, G., Palano, M., Tolomei, C., Gori, P. D., Calcaterra, S., Gambino, P., & Chiarabba, C. (2020). Flank sliding: A valve and a sentinel for paroxysmal eruptions and magma ascent at Mount Etna, Italy. *Geology*, *48*(11), 1077–1082. https://doi.org/10.1130/G47656.1

Poland, M. P., Peltier, A., Bonforte, A., & Puglisi, G. (2017). The spectrum of persistent volcanic flank instability: A review and proposed framework based on Kīlauea, Piton de la Fournaise, and Etna. *Journal of Volcanology and Geothermal Research*, *339*, 63–80. Elsevier B.V. https://doi.org/10.1016/j.jvolgeores.2017.05.004

Rovida, A., Locati, M., Camassi, R., Lolli, B., Gasperini, P., & Antonucci, A. (Eds.) (2021)., *Italian Parametric earthquake Catalogue (CPTI15), version 3.0*. Istituto Nazionale di Geofisica e Vulcanologia (INGV). https://doi.org/10.13127/CPTI/CPTI15.3

Ruch, J., Pepe, S., Casu, F., Solaro, G., Pepe, A., Acocella, V., et al. (2013). Seismo-tectonic behavior of the Pernicana fault system (Mt Etna): A gauge for volcano flank instability? *Journal of Geophysical Research: Solid Earth*, *118*(8), 4398–4409. https://doi.org/10.1002/jgrb.50281

Sambridge, M. (1999a). Geophysical inversion with a neighbourhood algorithm—I. Searching a parameter space. *Geophysical Journal International*, *138*(2), 479–494. https://doi.org/10.1046/j.1365-246X.1999.00876.x

Sambridge, M. (1999b). Geophysical inversion with a neighbourhood algorithm—II. Appraising the ensemble. *Geophysical Journal International*, *138*(3), 727–746. https://doi.org/10.1046/j.1365-246x.1999.00900.x

Siniscalchi, A., Tripaldi, S., Neri, M., Balasco, M., Romano, G., Ruch, J., & Schiavone, D. (2012). Flank instability structure of Mt. Etna inferred by a magnetotelluric survey. *Journal of Geophysical Research*, *117*(B3), B03216. https://doi.org/10.1029/2011JB008657

Trasatti, E., Giunchi, C., & Piana Agostinetti, N. (2007). Numerical inversion of deformation caused by pressure sources: Application to Mount Etna (Italy). *Geophysical Journal International*, *172*(2), 873–884. https://doi.org/10.1111/j.1365-246X.2007.03677.x

Tridon, M., Cayol, V., Froger, J. L., Augier, A., & Bachèlery, P. (2016). Inversion of coeval shear and normal stress of Piton de la Fournaise flank displacement. *Journal of Geophysical Research: Solid Earth*, *121*(11), 7846–7866. https://doi.org/10.1002/2016JB013330

Urlaub, M., Petersen, F., Gross, F., Bonforte, A., Puglisi, G., Guglielmino, F., et al. (2018). Gravitational collapse of Mount Etna's southeastern flank. *Science Advances*, *4*(10), eaat9700. https://doi.org/10.1126/sciadv.aat9700

Welstead, S. T. (1999). Fractal and wavelet image compression techniques. *The International Society for Optical Engineering*, *40*. https://doi.org/10.1117/3.353798

Wright, T. J., Parsons, B. E., & Lu, Z. (2004). Toward mapping surface deformation in three dimensions using InSAR. *Geophysical Research Letters*, *31*(1), L01607. https://doi.org/10.1029/2003GL018827